THIELE CENTRE
FOR APPLIED MATHEMATICS IN NATURAL SCIENCE

The saucor, a new stereological tool for analysing the spatial distributions of cells, exemplified by human neocortical neurons and glial cells

Anette K. Stark, Hans-Jørgen G. Gundersen,
Jonathan Gardi, Bente Pakkenberg and Ute Hahn

Research Report No. 13 | November 2009

The saucor, a new stereological tool for analysing the spatial distributions of cells, exemplified by human neocortical neurons and glial cells

Anette K Stark[1], Hans-Jørgen G Gundersen[2], Jonathan Gardi[2], Bente Pakkenberg[1], and Ute Hahn[3]

[1] *Research Laboratory for Stereology and Neuroscience, Bispebjerg University Hospital, Copenhagen, Denmark*

[2] *Stereology and Electron Microscopy Research Laboratory, University of Aarhus, Denmark*

[3] *Thiele Centre for Applied Mathematics in the Natural Sciences, Department of Mathematical Sciences, University of Aarhus, Denmark*

Abstract

The three dimensional spatial arrangement of particles or cells, for example glial cells, with respect to other particles or cells, for example neurons, can be characterized by the *radial number density function*, which expresses the number density of so called "secondary" particles as a function of their distance to a "primary" particle.

The present paper introduces a new stereological method, the *saucor*, for estimating the radial number density from thick isotropic uniform random (IUR) or vertical uniform random (VUR) sections. In the first estimation step, primary particles are registered in a disector. Subsequently, smaller counting windows are drawn with random orientation around every primary particle, and the positions of all secondary particles within the windows are recorded. The shape of the counting windows is designed such that a large portion of the volume close to the primary particle is examined and a smaller portion of the volume as the distance to the primary object increases. The experimenter can determine the relation between these volumina as a function of the distance by adjusting the parameters of the window graph, and thus reach a good balance between workload and obtained information. Estimation formulae based on the Horvitz-Thompson theorem are derived for both IUR and VUR designs.

The method is illustrated with an example where the radial number density of neurons and glial cells around neurons in the human neocortex is estimated using thick vertical sections for light microscopy. The results indicate that the glial cells are clustered around the neurons and the neurons have a tendency towards repulsion from each other.

1 Introduction

Biological tissue is not fully described by first order quantities like the mean number N_V of cells per volume, but also characterized by the spatial arrangement of cells. The necessity to quantify three-dimensional spatial relationships has been stated in many medical fields such as embryology (Chandebois, 1976), oncology (Mattfeldt *et al.*, 1993a,b), and diabetic nephropathology (Mayhew, 1999).

In the present paper, we analyse the spatial distribution of glial cells around neurons in different subregions of the human neocortex. According to the classical view of the nervous system, the more abundant glial cells play an inferior role in that they just provide an ideal environment for neuronal cell function. However, research has suggested that glial cells are intimately involved in the active control of neuronal activity and synaptic transmission. Any change in the spatial arrangement of glial cells with respect to the neurons may reflect functional changes in the relationship between them. Since the functions of the glial cell subtypes are different (Berry & Butt, 1997; Araque *et al.*, 1999; Ullian *et al.*, 2001), the spatial arrangement of glial cell subtypes around neurons should be expected to differ as well.

Since the methods presented below are not restricted to glial cells and neurons but can be applied to any kind of cells or particles, we will refer to the neurons as "primary" cells and to the glia as "secondary" cells in the following. This does not mean that primary and secondary particles necessarily have to belong to different types. In fact, we also analysed the distribution of neurons around other neurons in the practical part. The spatial distribution of secondary cells around primary cells is described by the so called *radial number density function* $N_{V\,12}$. The quantity $N_{V\,12}(r)$ can be understood as the average number of secondary cells in shells limited by spheres of radii $r - \delta$ and $r + \delta$ around arbitrarily picked primary cells, divided by the volume of the shell, with an infinitesimally small δ.

$N_{V\,12}$ is closely related to well known second order functions from the theory of spatial point processes. They are popular tools in the statistical analysis of spatial point patterns. Consequently, a rich literature exists on applications and estimation of these functions, for summaries see e.g. the books by Stoyan *et al.* (1995), Diggle (2003) or Illian *et al.* (2008). However, almost all applications concentrate on the two dimensional case. The few exceptions include the paper by Hanisch & Stoyan (1981), who propose a method for the stereological estimation of three dimensional second order functions from planar sections under the additional assumption that the particles or cells are spherical. The studies by Baddeley *et al.* (1987, 1993) investigate the spatial arrangement of osteocytes in bone by registering the positions within thick "bricks" with the help of a tandem scanning reflected light microscope. Jensen *et al.* (1990) provide a unified mathematical theory for the general n-dimensional case.

The need for tedious registration of the positions of cells or particles in thick bricks has probably been the main hamper to applying second order functions in the analysis of three dimensional structures. We therefore propose a new method that limits the sampling to thinner physical or optical sections, and moreover further reduces the data collection effort by restricting measurements to small subsets around primary cells. These subsets are called "saucors" after their shape. The

saucor sampling scheme extends (and corrects) earlier work of Evans & Gundersen (1989).

Saucor sampling can be used with isotropic uniformly random (IUR) sections as well as with vertical uniformly random (VUR) sections, thus enabling its application to tissue that is preferably examined by vertical sections, such as the brain. We provide estimation formula for the neighbour density function for both sectioning schemes. The estimators have been implemented in the Cast-GRID® software package (Visiopharm, Hørsholm, Denmark) for semi-automatic image analysis, which greatly facilitates the measurements and the computations.

A formal definition of the radial number density function is provided in Section 2, where we also discuss the relation of $N_{V\,12}(r)$ to other second order summary functions. The saucor sampling scheme and estimators for $N_{V\,12}(r)$ are introduced in Section 3. Section 4 is dedicated to the practical analysis of neocortical tissue. The paper concludes with a discussion in Section 5.

2 The radial number density function $N_{V\,12}$ and its relation to other second order summary functions

In order to describe the spatial arrangement of secondary particles with respect to primary particles, we will reduce the particles to points in the following. Thus we deal with the description of the mutual arrangement of two point patterns, representing primary and secondary particles. The average radial number density $N_{V\,12}(r_1, r_2)$ is defined as the expected number of secondary points with distance between r_1 and r_2 to an arbitrary random primary point, divided by the volume of the shell limited by spheres of radii r_1 and r_2, which is equal to $4/3\pi(r_2^3 - r_1^3)$:

$$N_{V\,12}(r_1, r_2) := \frac{\mathbf{E}\left[\begin{array}{c}\#\text{ secondary points within distance } r_1 \text{ and } r_2 \\ \text{to an arbitrary primary point}\end{array}\right]}{4/3\pi(r_2^3 - r_1^3)}. \qquad (1)$$

If the pattern of secondary points is completely independent of the primaries, $N_{V\,12}$ is constant and equal to the overall number density $N_{V\,2}$ of secondary particles. High values of $N_{V\,12}$ for small distances indicate clustering of secondary particles around primary particles. Conversely, repulsive behaviour results in small initial values of $N_{V\,12}$. In general, we will observe that $N_{V\,12}$ approaches $N_{V\,2}$ for large distances. When dealing with real particles or cells, $N_{V\,12}$ always vanishes for very small distances since cell or particle centres cannot come closer than the diameter of the cells or particles. The different cases of spatial interaction between primary and secondary particles are illustrated in Figure 1.

A continuous version of the radial number density of secondary points as a function of the distance to the primary is obtained by considering infinitesimally thin shells, limited by spheres of radii $r_1 = r - \delta$ and $r_2 = r + \delta$, namely

$$N_{V\,12}(r) := \lim_{\delta \to 0} N_{V\,12}(r - \delta, r + \delta). \qquad (2)$$

The functions $N_{V\,12}$ defined by equations (1) and (2) are closely related to the multivariate K-function K_{12} and the multivariate pair correlation function g_{12}.

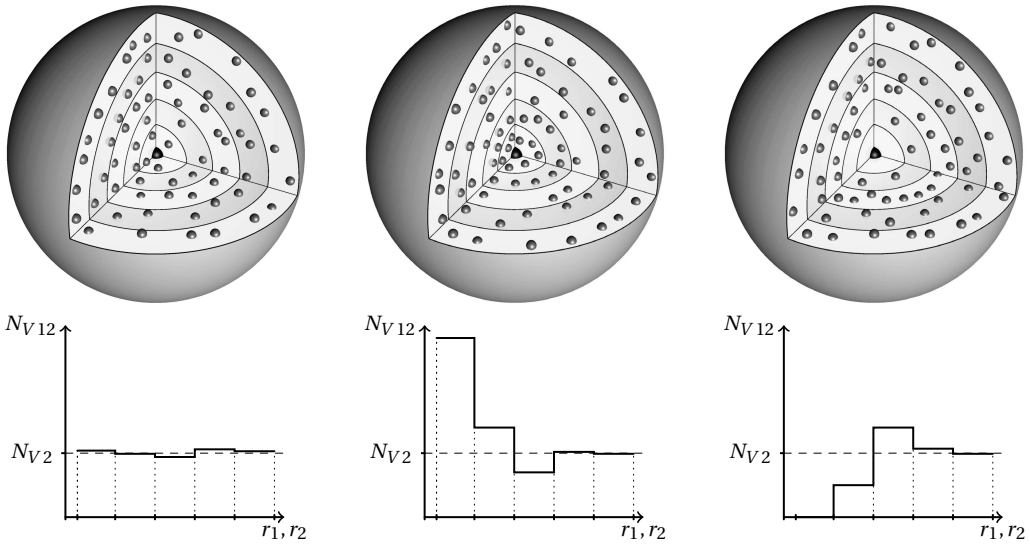

Figure 1: Spatial arrangement of particles with respect to other particles. Top: Example of a primary particle(dark) with surrounding secondary particles (light gray). Spherical shells with different distance to the primary are shaded in different gray levels. Bottom: Graph showing the piecewise constant version of the radial density $N_{V\,12}$ as given in Equation (1) corresponding to these shells. Left panel: completely random arrangement (Poisson case), middle: secondary particles cluster around the primary, right: repulsion between primary and secondaries.

These functions have a long standing tradition in the statistical analysis of stationary spatial point processes consisting of several types of points, for summaries see e.g. the books by Cressie (1993), Stoyan *et al.* (1995), Diggle (2003), or Illian *et al.* (2008). The bivariate K-function $K_{12}(r)$ is defined as the expected number of points of type 2 in a ball of radius r around a type 1 point, divided by the number density of type 2 points. In the setting of infinite stationary point processes, the K-function thus relates to $N_{V\,12}$ via

$$K_{12}(r) = \frac{N_{V\,12}(0, r) \cdot \frac{4}{3}\pi r^3}{N_{V\,2}}.$$

The derivative of the K-function, normalized by the surface area of a sphere of radius r, is the popular bivariate pair correlation function $g_{12}(r)$, and it is

$$g_{12}(r) = N_{V\,12}(r)/N_{V\,2}.$$

In recent years, a two dimensional version of $N_{V\,12}$, the so called Wiegand-Moloney ring statistic (Wiegand & Moloney, 2004), has furthermore become popular in ecology to describe the spatial arrangement of plants.

3 Estimation of radial number density using saucor sampling

3.1 The general estimation principle for $N_{V\,12}(r_1, r_2)$

The radial number density $N_{V\,12}$ is defined as the *expected* number density of secondary particles around an *arbitrary* primary particle, which means that all primary

particles contribute by the same amount to $N_{V\,12}$. Therefore we start by sampling primary particles with equal probability. This is achieved using a disector design (Sterio, 1984) which combines uniform random thick sections with a systematic uniform random positioned unbiased counting frame. In the second step, the number of secondary particles in the shell with radius between r_1 and r_2 around each sampled primary is separately estimated from the same thick section using an efficient unbiased estimator that is described in detail below. This second estimator requires that the thick sections be uniformly randomly orientated. Depending on the situation, the experimenter may choose either isotropic uniform random sections (IUR, randomly rotated around two axes) or vertical uniform random sections (VUR, randomly rotated around an identifiable axis, see Baddeley *et al.* (1987)).

The estimator for $N_{V\,12}$ is then simply obtained by averaging over the individual results. Formally, let n denote the number of primary particles sampled in the first step, and $\widehat{N}_2(c_i; r_1, r_2)$ be the estimated number of secondary particles with distance between r_1 and r_2 to the ith primary particle located in point c_i, then the proposed estimator reads

$$\widehat{N}_{V\,12}(r_1, r_2) = \frac{1}{n} \sum_{i=1}^{n} \frac{\widehat{N}_2(c_i; r_1, r_2)}{4/3\,\pi(r_2^3 - r_1^3)}. \tag{3}$$

Since the primary particles are sampled with equal probability and their number n is random, the estimator $\widehat{N}_{V\,12}(r_1, r_2)$ is *ratio* unbiased. A thorough discussion on estimators of the form (3) for particle populations can be found in the excellent book by Baddeley & Jensen (2005).

We now turn to the unbiased estimation of the number $N_2(c_i; r_1, r_2)$ of secondary particles around the i-th primary. In order to find out whether or not a secondary particle found in the thick section lies within distance between r_1 and r_2 to the given primary, its three dimensional coordinates have to be recorded. As mentioned before, particles are reduced to associated points for distance measurement; we will refer to these points as to the particles centres in the following.

If all observable secondary particles were evaluated, one would have to perform many more measurements in shells with large radii than in shells close to the primary centre c_i. By simple calculation one finds the number of secondary cells in the thick section at a distance between $r - \delta$ and $r + \delta$ to the primary to be roughly proportional to r. Moreover, the spatial distribution of secondary particles far away from the primary is expected to be less informative from a biological point of view. It is therefore desirable to reduce the measurement effort associated with the estimation of $N_{V\,12}(r)$ for larger values of r. This is achieved by restricting the counting of secondaries to a subset of the observation field, the *saucor graph* described in Section 3.3.

This graph is drawn individually with random orientation in the observation plane for every primary particle; we denote the graph belonging to the i-th primary by W_i. A secondary centre c_j is thus only sampled for the estimation of $N_2(c_i; r_1, r_2)$ if it lies both in the (randomly orientated) thick section T and in the (randomly orientated) saucor graph W_i. The probability that c_j is sampled as a "satellite" of the the primary c_i factorizes into the probability

$$p_{\text{sect}}(c_j; c_i) := \text{Prob}(c_j \text{ lies in } T \,|\, T \text{ contains } c_i)$$

that the j-th secondary is observed in the thick section if the i-th primary has been observed, and the probability

$$p_{\mathrm{sau}}(c_j; c_i) := \mathrm{Prob}(c_j \text{ lies in } W_i \,|\, T \text{ contains } c_i \text{ and } c_j)$$

that c_j falls into the saucor graph around c_i. The probability p_{sect} depends on the type of orientation randomization (IUR or VUR) for the thick section sampling; we distinguish between p_{Isect} and p_{Vsect} correspondingly. Formulae are given for both cases in Subsection 3.2. Subsection 3.3 is devoted to the saucor graph and to the calculation of p_{sau}.

Following the Horvitz-Thompson principle (Horvitz & Thompson, 1952), we now obtain an unbiased estimator of the total number $N_2(c_i; r_1, r_2)$ of secondary centres around the primary by weighting the individual counts with the inverse of the sampling probability $p_{\mathrm{sect}}(c_j; c_i) \cdot p_{\mathrm{sau}}(c_j; c_i)$, that is,

$$\widehat{N}_2(c_i; r_1, r_2) = \sum_{\substack{\text{sec. centres} \\ c_j \in T \cap W_i}} \frac{\mathbf{1}(r_1 < \mathrm{dist}(c_j, c_i) \le r_2)}{p_{\mathrm{sect}}(c_j; c_i) \cdot p_{\mathrm{sau}}(c_j; c_i)} \tag{4}$$

where $\mathrm{dist}(c_j, c_i)$ stands for the Euclidean distance between the secondary point c_j and the primary point c_i, and the indicator function $\mathbf{1}$ is used to count the secondary points with distance between r_1 and r_2 to the primary c_i,

$$\mathbf{1}(r_1 < \mathrm{dist}(c_j, c_i) \le r_2) = \begin{cases} 1, & r_1 < \mathrm{dist}(c_j, c_i) \le r_2, \\ 0, & \text{otherwise.} \end{cases}$$

By combining (3) with (4), the estimation procedure finally boils down to the following recipe:

1. Take a uniform random thick section (VUR or IUR) of the containing organ or reference space (the section can also be an optical section, and guard zones may be required, see the remark below).

2. Position a counting frame on the section, identify the primary particles therein, and record the 3D positions of their centres (associated points). Let n denote their number and $c_1, \ldots c_n$ denote their centres.

3. For every centre c_i, estimate the number of surrounding secondary particles as follows:

   (a) According to the instructions in subsection 3.3, make a randomly orientated saucor graph W_i around c_i on the observation window or screen.

   (b) Identify the secondary particle centres within the thick section T that fall into W_i and record their positions.

   (c) For every sampled secondary centre c_j, calculate the probability $p_{\mathrm{sect}}(c_j; c_i)$ using formula (6) in the case of IUR sections or (8) in the case of VUR sections, and find the probability $p_{\mathrm{sau}}(c_j; c_i)$ from (11).

   (d) Apply formula (4) to get the estimate $\widehat{N}_2(c_i; r_1, r_2)$.

4. Obtain an estimate for the radial number density by averaging the results from step 3 according to formula (3).

Remark: Although secondary particles or cells are counted by means of an associated point such as the nucleolus centroid, they do have a spatial dimension. This causes problems with counting particles close to the physical thick section boundaries — for example, particles may get lost due to the sectioning process, and for those that are hit by the section boundary, it is not clear whether or not their associated centre falls within the section. Similar problems also affect the disector counting of primary particles. Therefore we equip the original physical section with an upper and a lower guard zone, as recommended by Andersen & Gundersen (1999). These guard zones actually reduce the original thick section of thickness $h_{\text{original section}}$ to an optical thick section of thickness (or height)

$$h := h_{\text{original section}} - (h_{\text{upper guard zone}} + h_{\text{lower guard zone}}).$$

In what follows, we will always identify the section plane with the xy-plane and the focal depth with the z-coordinate. Thus the xy-plane is identical with what is seen on the microscopical screen. If the section is vertical uniform random, the direction of the y-axis is as usual set to the vertical direction.

3.2 UR section sampling

Saucor sampling starts with an UR *thick* section T of height h that is bounded by two parallel UR planes. Uniform random (UR) sectioning consists in a jointly uniform randomization of direction and position of the section plane. The direction is represented by the normal vector, and the position by the distance to the origin. For IUR sections, the normal vector takes values the whole unit sphere (all directions in three dimensions). VUR sections are parallel to a predefined vertical direction that is often given by the situation Baddeley *et al.* (1986). VUR section is necessary, for example, when substructures in certain organs are only easy to identify if the organ is cut perpendicular to its surface. This perpendicular plane is called the "horizontal plane". For a mathematical description of IUR and VUR sectioning see e.g. Baddeley & Jensen (2005).

In the following, we will give heuristical derivations of the conditional probability $p_{\text{sect}}(c_j; c_i)$ for observing a secondary point c_j in the section given the primary point c_i has fixed distance $d_i \leq h/2$ to the closer one of the two section boundary planes. One might object that this condition is somewhat stronger than the condition "T contains c_i" used in the previous definition of $p_{\text{sect}}(c_j; c_i)$ in subsection 3.1. However, this does not infringe the unbiasedness of the estimator $\widehat{N}_2(c_i; r_1, r_2)$ as given by (4). We will always let x_i, y_i, z_i denote the coordinates of a point c_i representing the primary particle centre and x_j, y_j, z_j the coordinates of the secondary particle centre c_j as measured under the digitally equipped microscope.

IUR sections. IUR sampling is designed such that all points in the reference space have equal probability to be contained in the IUR thick section. However, if we fix a point c_i and condition on that point being contained in the section T, we

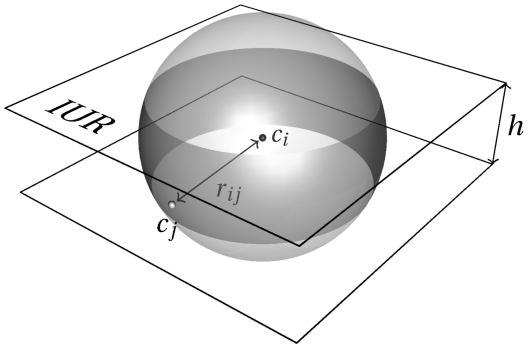

Figure 2: IUR sampling. Section centred on a primary particle marked as black dot. Of all secondary particles with the same distance to the primary as the one marked with a light dot, only those who lie in the dark shaded surface are sampled by this section. Due to the isotropic uniform randomization of the section, all points on the sphere are sampled with equal probability corresponding to the fraction of the dark shaded part in the surface area of the whole sphere.

will sample points that are close to c_i with higher probability than points further away.

Due to the isotropic rotation of T, all points on a sphere with fixed radius around c_i are sampled with the same conditional probability. This probability is therefore equivalent to the fraction of the sphere surface which is contained in the section, as illustrated in Figure 2.

Consequently, the probability $p_{\text{Isect}}(c_j; c_i)$ is a function of the distance r_{ij} between c_i and c_j,

$$r_{ij} := \sqrt{(x_i - x_j)^2 + (y_i - y_j)^2 + (z_i - z_j)^2}. \tag{5}$$

The surface area of the spherical layer in T is equivalent to $2\pi r_{ij} h^*$, where h^* is the height of the spherical layer, which also depends on the distance d_i of c_i to the section boundary, see Figure 3.

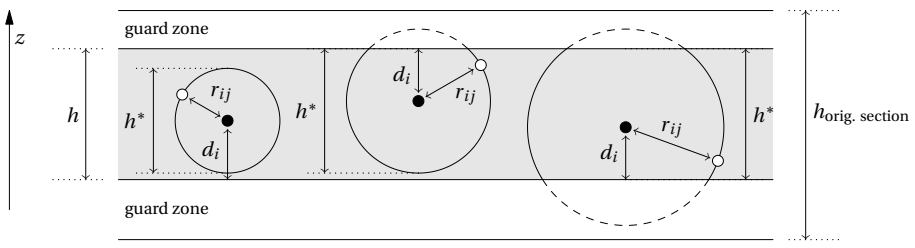

Figure 3: IUR conditional sampling probability $p_{\text{Isect}}(c_j; c_i)$ depends on d_i and r_{ij}. IUR section (with guard zones) viewed edge on in the plane that contains both c_i and c_j, that is, the sphere around c_i (black dot) through c_j (white) is cut centrally. h^* denotes the height of the spherical layer within the section. Points c_j with $r_{ij} \leq d_i$ are sampled with probability 1, because the whole sphere is contained in the section (left part). If $d_i < r_{ij} \leq h - d_i$, more than a entire half of the sphere is contained in the section (middle), otherwise if $r_{ij} > h - d_i$, the sphere is cut on both sides (right part).

The resulting probability is

$$p_{\mathrm{Isect}}(c_j; c_i) = \frac{\text{Area(sphere around } c_i \text{ with radius } r_{ij} \cap \text{thick section)}}{\text{Area(sphere with radius } r_{ij})} = \frac{2\pi r_{ij} h^*}{4\pi r_{ij}^2}$$
$$= \begin{cases} 1, & r_{ij} \le d_i, \\ \frac{1}{2}(1 + d_i/r_{ij}), & d_i < r_{ij} < h - d_i, \\ h/(2r_{ij}), & r_{ij} \ge h - d_i. \end{cases} \tag{6}$$

VUR sections. Just as IUR sections, also VUR sections sample all points in the reference space with equal probability. Again, we condition on the case that the point c_i which represents the primary has a given distance d_i to the closer one of the two boundary planes of the section. The VUR sections that fulfill this condition are obtained by uniform rotation around the vertical axis through c_i. This implies that all secondary points with the same given distance to that axis are sampled with the same probability $p_{\mathrm{Vsect}}(c_j; c_i)$. These points lie on a cylinder, as shown in Figure 4. The sampling probability corresponds to the fraction of the cylinder surface which is contained in the thick section. Therefore, $p_{\mathrm{Vsect}}(c_j; c_i)$ depends on the distance

$$r_{ij}^{(xz)} := \sqrt{(x_j - x_i)^2 + (z_j - z_i)^2} \tag{7}$$

of c_j to the vertical axis through c_i (recall that the vertical direction is identified with the y-direction in the microscopical section, and the horizontal plane perpendicular to this direction is the (xz)-plane).

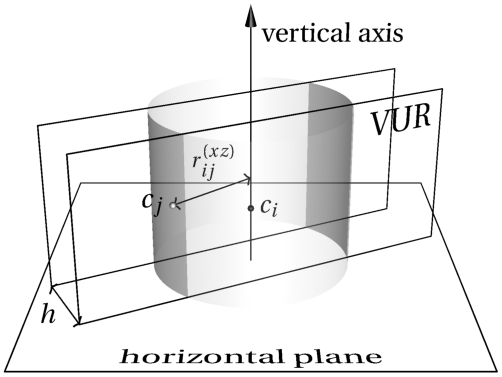

Figure 4: VUR sampling. Section centred on a primary particle c_i marked as black dot. Due to the vertical uniform randomization of the section, secondary points with equal conditional sampling probability p_{Vsect} are located on cylinders around the vertical axis through c_i. The sampling probability corresponds to the fraction of the dark shaded part in the surface area of the whole cylinder. The distance of a point c_j to the vertical axis does not depend on its vertical (y-) coordinate.

Since cylinder surface is obtained by multiplying the length of the profile on the horizontal plane with the cylinder height, the cylinder surface fraction within the section equals the the length fraction of the circle with radius $r_{ij}^{(xz)}$ around the horizontal projection of c_i that is covered by the horizontal profile of the thick

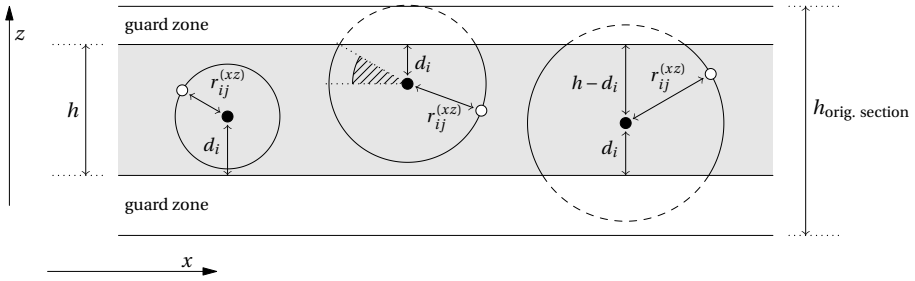

Figure 5: VUR conditional sampling probability $p_{\mathbf{Isect}}(c_j; c_i)$ depends on d_i and $r_{ij}^{(xz)}$. The projections of the VUR thick section (with guard zones) and the cylinders as in Figure 4 onto the horizontal plane are shown, that is, the vertical axis is perpendicular to the paper, and the black and white dots represent the projections of primary and secondary point c_i and c_j, i.e., their x- and z- coordinates. Points c_j with $r_{ij}^{(xz)} \leq d_i$ are sampled with probability 1 (left part). The calculation of the sampling probability in the case $r_{ij}^{(xz)} > d_i$ requires determination of arc lengths — the hatched angle in the middle part is equal to $\arcsin\left(d_i / r_{ij}^{(xz)}\right)$.

section, see Figure 5. Thus, the probability $p_{\text{Vsect}}(c_j; c_i)$ is given by

$$
\begin{aligned}
p_{\text{Vsect}}(c_j; c_i) &= \frac{\text{Length(circle in } xz\text{-plane around } c_i \text{ with radius } r_{ij}^{(xz)} \cap \text{section)}}{\text{Length(circle with radius } r_{ij}^{(xz)})} \\
&= \begin{cases} 1, & r_{ij}^{(xz)} \leq d_i, \\ \frac{1}{2} + \frac{1}{\pi} \arcsin\left(d_i / r_{ij}^{(xz)}\right), & d_i < r_{ij}^{(xz)} < h - d_i, \\ \frac{1}{\pi}\left[\arcsin\left((h-d_i)/r_{ij}^{(xz)}\right) + \arcsin\left(d_i / r_{ij}^{(xz)}\right)\right], & r_{ij}^{(xz)} \geq h - d_i. \end{cases}
\end{aligned} \tag{8}
$$

3.3 The saucor

The idea of the saucor sampling method is to restrict coordinate measurement for secondary particles to independently randomly orientated observation windows W_i, drawn on the microscopy screen around the individual primary particles c_i, $i = 1, \ldots, n$, as shown on Figures 7 and 8. Once the random orientation of the window is established for a given primary c_i, it remains fixed across focal depths. A secondary particle c_j is counted (or measured) with c_i if its x- and y- coordinates fall into W_i, no matter what its z-coordinate is. The window is limited to points with distance less or equal to $R_{\max}$ to the centre c_i. This radius is chosen by the experimenter as the upper limit of biological interest for the determination of $N_{V\,12}$. On the other hand, the window contains all points with distance less or equal to a user determined R_{mid}. In the neuroanatomical study presented in Section 4 we chose $R_{\text{mid}} = 12\,\mu\text{m}$ and $R_{\max} = 48\,\mu\text{m}$.

The shape of W_i is defined by Equation (9) in polar coordinates r and θ, where r denotes the distance in the focal plane to the centre point of W_i, and θ denotes the (planar) angle to the axis of W_i. A point with polar coordinates (r, θ) belongs to the W_i if and only if $|\theta| \leq \theta(r)$, and $r \leq R_{\max}$, where

$$
\theta(r) = \begin{cases} \pi, & r \leq R_{\text{mid}}, \\ \pi\left(\frac{R_{\text{mid}}}{r}\right)^{1+\beta}, & r > R_{\text{mid}}. \end{cases} \tag{9}
$$

The parameter β determines how many of the secondary particles with distance larger than R_{mid} to the primary have to be counted and how fast this number decreases. Figure 6 shows the graph of W_i for various values of β in the case where the axis of W_i coincides with the x-axis. For the practical example, we chose $\beta = 1$. The name "saucor" was inspired by the shape that is obtained if the graph in Figure 6 were rotated around the y-axis.

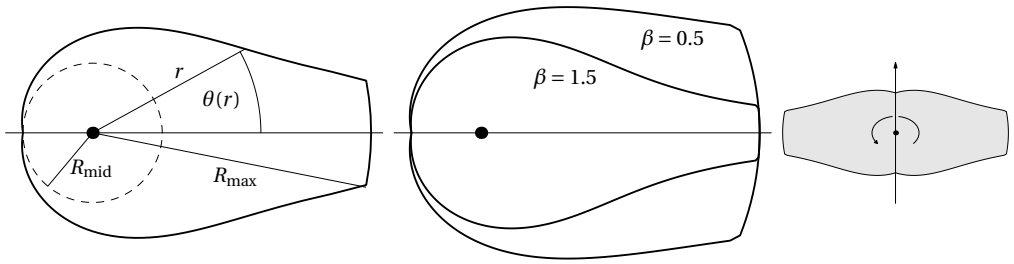

Figure 6: The saucor graph, here oriented along the x-axis. Left part: saucor graph for $\beta = 1$, middle: saucor graphs for $\beta = 0.5$ (outer) and $\beta = 1.5$ (inner graph). Right: rotation of the graph around the vertical axis through the primary would produce a shape that resembles a flying saucer.

Randomization of the saucor orientation is performed by uniform rotation of the saucor axis around the primary particle. The probability $p_{\text{sau}}(c_j; c_i)$ that a secondary point c_j with coordinates x_j, y_j as seen on the microscopy screen lies inside the graph therefore depends only on the xy- (or screen-) distance $r_{ij}^{(xy)}$ to the primary with coordinates x_i, y_i,

$$r_{ij}^{(xy)} := \sqrt{(x_j - x_i)^2 + (y_j - y_i)^2}. \tag{10}$$

This probability is given by the length fraction of the arc through c_j in the saucor window, see Figure 7,

$$\frac{\text{Length(circle around } c_i \text{ with radius } r_{ij}^{(xy)} \cap \text{saucor graph)}}{\text{Length(circle with radius } r_{ij}^{(xy)})} = \frac{2\theta(r_{ij}^{(xy)}) \cdot r_{ij}^{(xy)}}{2\pi \cdot r_{ij}^{(xy)}},$$

that is,

$$p_{\text{sau}}(c_j; c_i) = \begin{cases} 1, & r_{ij}^{(xy)} \le R_{\text{mid}}, \\ \left(R_{\text{mid}}/r_{ij}^{(xy)}\right)^{1+\beta}, & R_{\text{mid}} < r_{ij}^{(xy)} \le R_{\text{max}}. \end{cases} \tag{11}$$

Note that the saucor estimator holds only for $N_{V\,12}(r)$ with $r < R_{\text{max}}$. Very few secondary particles may be observed on the edge of the saucor graph with three dimensional distance r_{ij} larger than R_{max}, since the screen distance is in general smaller than the true three dimensional distance, namely

$$r_{ij}^{(xy)} = \sqrt{r_{ij} - (z_i - z_j)^2}. \tag{12}$$

These particles normally constitute less than 1 % of all measured particles and are excluded from the computation.

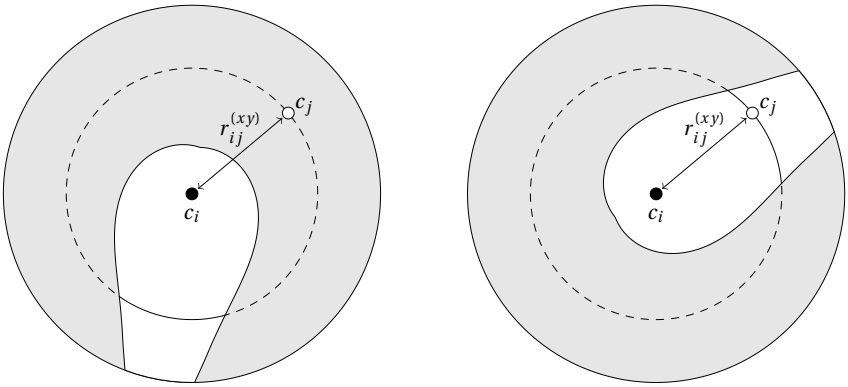

Figure 7: Random rotation of the saucor graph around the primary point. Two realizations of the uniformly rotated saucor graph as drawn on the screen are shown, see also Figure 8. Secondary cells are only sampled when they fall into the white area.

3.4 Number of measurements associated with saucor sampling

The workload associated with measuring particle coordinates in a thick section is roughly proportional to the expected number of particles in the evaluated volume. Traditional methods capture all secondary particles that can be seen by focussing up and down in a given counting frame. The expected number $\mathbf{E}Q(\text{disector box})$ of secondary particles depends on the area of the frame, the height h of the section and the number density $N_{V\,2}$, namely

$$\mathbf{E}Q(\text{disector box}) = N_{V\,2} \cdot \text{Area(frame)} \cdot h. \tag{13}$$

When sampling secondaries individually for every primary, the effort increases with the number of primary particles in the disector box. For the saucor method, one has to evaluate cylinder volumes that equal the area of the saucor graph multiplied by the height h. This yields an expected number $\mathbf{E}Q(\text{saucor})$ of secondary counts given by

$$\mathbf{E}Q(\text{saucor}) = N_{V\,2} \cdot \#\text{primaries} \cdot \text{Area(saucor)} \cdot h. \tag{14}$$

Thus, saucor sampling will require less measurement effort than disector sampling if and only if #primaries < Area(frame)/Area(saucor).

Using the standard formula for the area swept out by a radius-vector function, we find

$$\begin{aligned}
\text{Area(saucor)} &= \int_0^{R_{\max}} 2\theta(r) r \,\mathrm{d}\, r \\
&= \pi R_{\text{mid}}^2 + \int_{R_{\text{mid}}}^{R_{\max}} 2\pi r^{-\beta} R_{\text{mid}}^{1+\beta} \,\mathrm{d}\, r \\
&= \pi R_{\text{mid}}^2 \cdot \begin{cases} 1 + 2\log \frac{R_{\max}}{R_{\text{mid}}}, & \text{if } \beta = 1, \\ -\frac{1+\beta}{1-\beta} + \frac{2}{1-\beta}\left(\frac{R_{\max}}{R_{\text{mid}}}\right)^{1-\beta}, & \text{otherwise.} \end{cases}
\end{aligned} \tag{15}$$

In the following neuroanatomical study, a saucor graph was used with $\beta = 1$, $R_{\text{mid}} = 12\,\mu\text{m}$ and $R_{\max} = 48\,\mu\text{m}$, having area $1707\,\mu\text{m}^2$.

4 Practical application: Estimating radial number density around neurons in the human neocortex in VUR sections

4.1 Tissue and tissue preparation

To illustrate the saucor method we analysed vertically uniformly random neocortical sections. The post mortem tissue consisted of one hemisphere from a 61-year-old woman who had no history of psychiatric or neurological disorders and died of cardiac arrest. The brain was removed from the calvarium within 72 hours of death and fixed in 0.1 M sodium phosphate buffered (pH 7.2) 4 % formaldehyde for 5 months. The meninges were removed, and the cerebellum and brainstem detached at the level of the third cranial nerve. The frontal, temporal, parietal and occipital regions were delineated and indicated by applying different colours to the pial surface of the right hemisphere Pakkenberg & Gundersen (1997). The hemisphere was embedded in 6 % agar, and sliced coronally at 7 mm-intervals, and the neocortical volume of the sliced hemisphere was estimated by Cavalieri's principle. From every second slice, using a special sampling plate, transcortical wedges were sampled uniformly and systematically random from each neocortical region. Each wedge was cut into 2 mm-wide parallel bars. Each subsampled bar was rotated randomly around its vertical axis and embedded in LKB-historesin. One 35 µm-thick vertical section was cut from each block, and stained with a modified Wolbach's Giemsa stain. This resulted in a set of thirty-three 35 µm-thick vertical Giemsa stained sections; nine frontal, ten temporal, eight parietal and six occipital bars, which were mounted on glass slides for microscopic examination.

4.2 Equipment

The slides were placed on the stage of a BH-2 Olympus microscope. The slide holder could be freely rotated to enable sampling along the direction of the vertical axis of the section. The image of the section was captured by a digital video camera and transmitted to a computer screen. A high image resolution and a thin focal plane was obtained using a high numerical aperture (NA = 1.4), 100× oil-immersion objective for cell counting and cell volume estimation. A Heidenhein microcator with digital readout for measuring movements to the nearest 0.5 µm kept track of the z-direction. The stage of the microscope and hence the specimen could be moved precisely in x, y, and z-directions and its movements were tracked and recorded. The position of the cursor was also tracked and 3D coordinates of the points marked with the cursor were recorded automatically. The final magnification at the computer screen was 3040X.

The volume of each sampled neuron was estimated by the vertical planar rotator method using the CAST-GRID computer-program (Visiopharm, Hørsholm, Denmark), which also controlled all data acquisition from the saucor.

4.3 Data acquisition

The primary neurons were identified in an optical disector (Gundersen et al., 1988) with a disector area of 3500 µm^2 and a disector height of 10 µm (from 10 µm to 20 µm

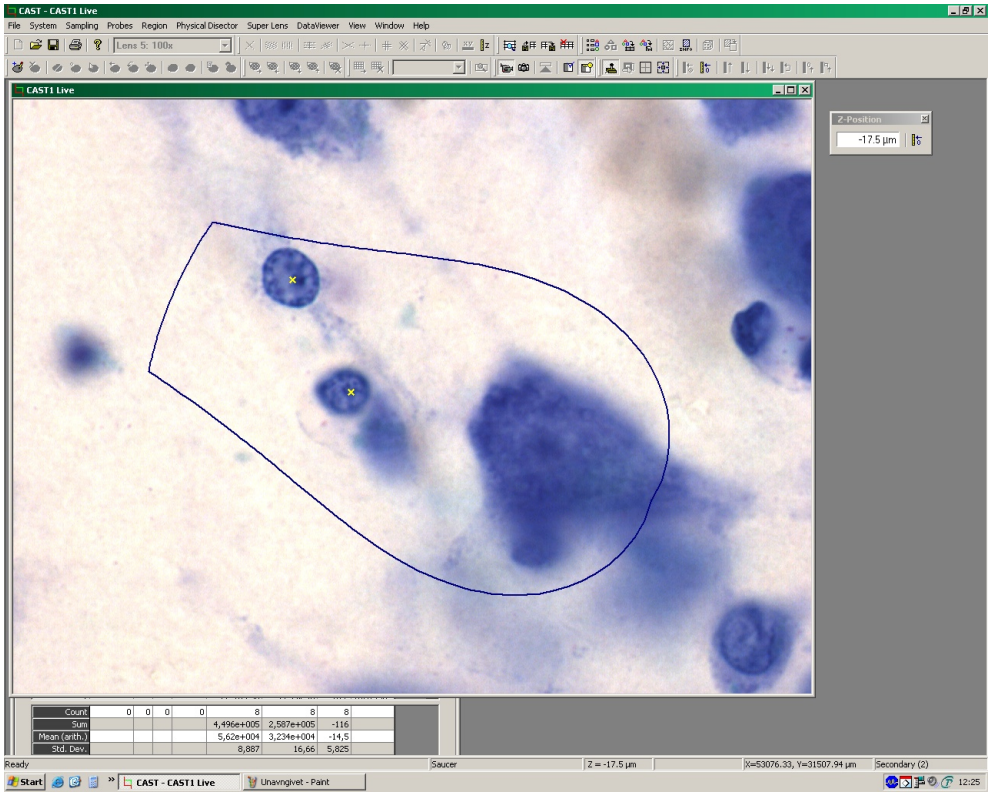

Figure 8: The saucor probe on the live screen, the focal plane of the image is several µm below the central focal plane centred on the nucleolus of a neuron. Two glial cells are sampled (yellow X), the upper one in this focal plane. The width of the field of view is ca. 80 µm.

leaving 10 µm thick guard zones on each side). Then the saucor was applied (see details below). The dimensions of the saucor were defined by $\beta = 1$, $R_{\text{mid}} = 12\,\mu\text{m}$ and $R_{\text{max}} = 48\,\mu\text{m}$. An example of the saucor on the screen is shown in Figure 8.

The secondary cells were classified on cytoarchitectonic characteristics into neurons, oligodendrocytes, astrocytes, microglial or endothelial cells. Cell classification was based solely on morphology because immunohistochemical staining cannot penetrate the plastic sections. The cells were identified as neurons if they had a combination of a single large nucleolus free of any surrounding heterochromatin, a typical pale chromatin pattern in a triangularly rounded nucleus, and were surrounded by a visible cytoplasm. Astrocytes were defined as cells with a round and pale nucleus having the heterochromatin concentrated in granules in a rim below the nuclear membrane and a relatively translucent cytoplasm. A small nucleolus was not always identified, but when present, it was most often situated eccentrically. The nuclear membrane of astrocytes has a sharp profile, and the cells are often located singularly. Oligodendrocytes are often situated in groups and in close proximity to neurons or blood vessels. They are characterized by a small rounded or oval nucleus with dense chromatin structure and a perinuclear halo. Microglia cells are defined by a small elongated or comma-shaped nucleus with dense peripheral chromatin.

A total of 151 primary neurons were sampled for the the estimation of radial number density, 32 in the frontal region, 49 in the temporal, 37 in the parietal and 33 in the occipital lobe. This means that an aggregate saucor area of

$151\,\mu m \times 1707\,\mu m = 257\,757\,\mu m^2$ had to be scanned for secondary cells. The traditional disector box counting methods would have required to inspect all disectors containing primary neurons. Since 100 of the 120 disectors that were screened did contain neurons, this would correspond to an area of $100 \times 3500\,\mu m^2$, which is about 36 % larger than the aggregate saucor area.

4.4 The practical use of the Saucor and the final computations

First the direction of the vertical axis was indicated, in this case the longitudinal axis of the sections. With a random start, the sampling of primary cells was performed with a constant sampling period of 1500 µm between the disectors along the centre of the section. All primary neurons in a disector must be sampled to ensure uniform sampling.

When the centre of a primary cell is indicated with the mouse in the relevant frame, the system moves the table so that the primary is at $(0, 0)$, and a saucor probe is drawn, rotated uniformly random, cf. Figure 8. The user indicates all secondary cell centres that in any way touch the saucor graph. At this stage the borders of the shells are concealed for the investigator. Coordinates (x, y, z) are automatically recorded for primary and secondary cells. When sampling in a saucor probe is exhausted, the investigator activates the rotator probe to estimate the volume of the primary neuron. This procedure is done for all primary neurons within a disector.

For simplification we have described the primary cells as neurons and secondary cells as glial cells. One can off cause pick any type of cell or other objects to be defined as primary or secondary, the same type of object can also be defined as both primary and secondary. For this practical application we chose primary cells to be neurons and both neurons and glial cells as secondary cells.

4.5 Data analysis and results

We present the radial number density of neocortical cells around primary neurons as a sequence sorted according to radial distance. The distance is classified or binned based on the observed radii, r_{ij}. It is most efficient to use a binning that reflects the inverse density of observations as the statistical properties of such estimates are mostly governed by the roughly constant number of observations in each class and the total number of observations; therefore the width of the individual classes reflects the observation density in that specific class (if the spatial distribution were uniform). In short: wide classes at the perimeter to obtain enough observations in the decreasing observed shell volume fractions and narrow classes in the centre and its vicinity to ensure precision and details of the interesting part of the distribution.

Unless many observations are made (>200), there is no extra information in more than roughly ten informative classes. Since there will often be some empty and thereby uninformative classes in the centre (the beginning of the distribution will often start some distance from the primary object centre) a few extra classes are needed to end up with about ten informative classes; we have chosen $n = 14$.

Finally, secondary particle centres cannot be arbitrarily close to that of the primary, so we have fixed the beginning of the sequence of bins at $R_1 = 2.4\,\mu m$. The binning is a refined geometric progressing or quasi-logarithmic sequence of classes,

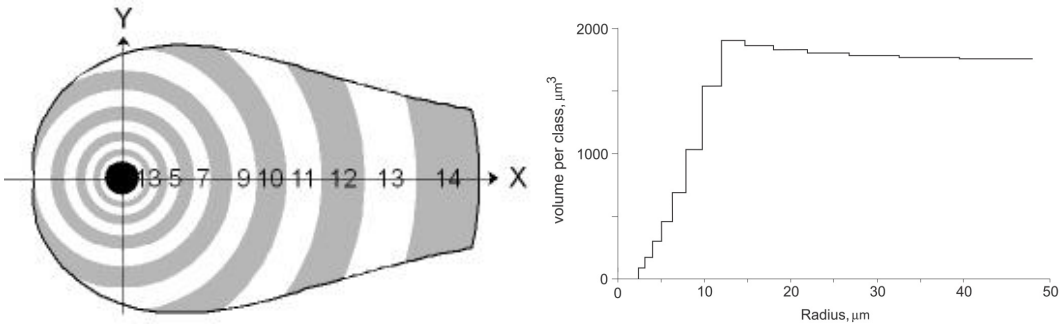

Figure 9: Binning of the saucor. Left panel: Profile of the binned saucor. In the central black circle secondary particle centres are excluded due to the presence of the primary cell. Right panel: The volume per bin of a saucor with a thickness of 10 µm.

which provides freedom to make it fit the three constants R_1, R_{mid}, and R_{max} (in a logarithmic sense it is symmetric around R_{mid}). The generating equation for the complete sequence of lower bin limits is

$$R_i = c \cdot f^{i-1} - \mathit{off} = 3.490 - 1.20783^{i-1} - 1.09, \tag{16}$$

where

$$c = \frac{(R_{\mathrm{mid}} - R_1)^2}{R_{\mathrm{max}} - 2R_{\mathrm{mid}} + R_1}, \tag{17}$$

$$f = \left[\frac{R_{\mathrm{mid}} - R_1}{c} + 1\right]^{2/n} \tag{18}$$

and

$$\mathit{off} = c - R_1. \tag{19}$$

The factor of geometric progression, $f \approx 1.21$, means that each class is 21 % wider than the previous one, providing an essentially constant sampling volume per bin outside of R_{mid}, as shown in Figure 9.

For each neocortical region the numerical density in each saucor shell was calculated for secondary cells: neurons divided into three volume groups and glial cells divided into astrocytes, oligodendrocytes and microglial cells. This produced a heavy data load, here we present the summarized data in plots where the abscissa is the volume of the spheres in the surface of which each secondary cell is situated, and the ordinate is the secondary cell density.

Figure 10 illustrates the difference in the spatial arrangement of glial cells and neurons with respect to (primary) neurons by comparing the radial glial and neuron number density averaged over all four regions. The graph for glial cells shows a pattern with high densities close to the neurons and a gap with lower density before the background density is reached, thus indicating clustering of glia around neurons. On the contrary, the radial density of neurons around neurons is small for small distances and approaches the final density from below. This suggests a tendency towards repulsion from the primary neuron.

We have chosen to illustrate the distribution of all cells around neurons with the four subdivisions (frontal, temporal, parietal, and occipital cortex) with the distribution in neocortex in the same graphs to make the regional differences more

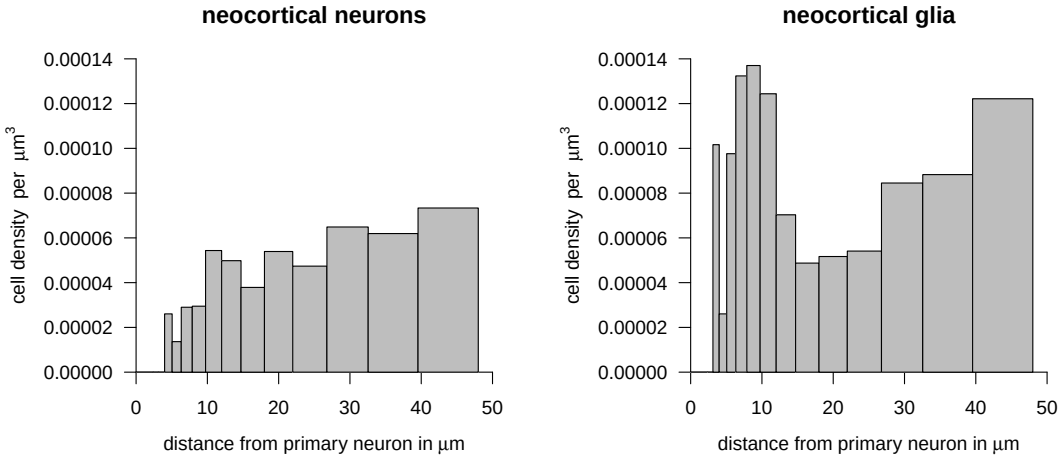

Figure 10: Radial number density of neurons and glial cells in the neocortex as a function of the distance from neurons, averaged over all four neocortical regions.

visible (see Figure 11). For estimating total radial number density of neocortical cells, each region is weighted with the fraction of the total number of neurons in that specific region. It is a very limited sample but there is a tendency towards glial attraction in all four regions, the glial cells are distributed in the same pattern over the four neocortical regions. The distribution of secondary neurons on the other hand presents a difference in the density when comparing the pattern of the frontal region to the other regions, probably due to the simple fact that the neurons in the frontal cortex have a larger volume than the neurons in the other regions.

For this study the embedding material was historesin, which has low shrinkage potential, unlike paraffin or frozen sections, for example. For studying spatial distribution of cells it is important to choose an embedding material with as little shrinkage potential as possible. Frozen and vibratome sections are special in that it is usually possible to restrict the shrinkage to the z-axis, and that is easily monitored locally Dorph-Petersen *et al.* (2001). If the sections are cut using a calibrated microtome one may then correct for the local shrinkage of the z-coordinate.

5 Conclusions

The spatial distribution of neurons in relation to other nearby neurons is of interest because the distribution of cells within a given region of the brain may have important implications for the function of that region. The ability of an ensemble of neurons to work in a coordinated fashion depends on the intensity of its synaptic connectivity, which in turn may be reflected in the physical proximity or arrangement of the cells. Spatial arrangement of cells or particles with respect to each other is suitably characterized by the radial number density which expresses the local mean number per volume of cells of one type as a function of their distance to cells of another (or the same) type. With this paper, we introduce a stereological probe, the saucor that allows efficient sampling and estimation of the radial number

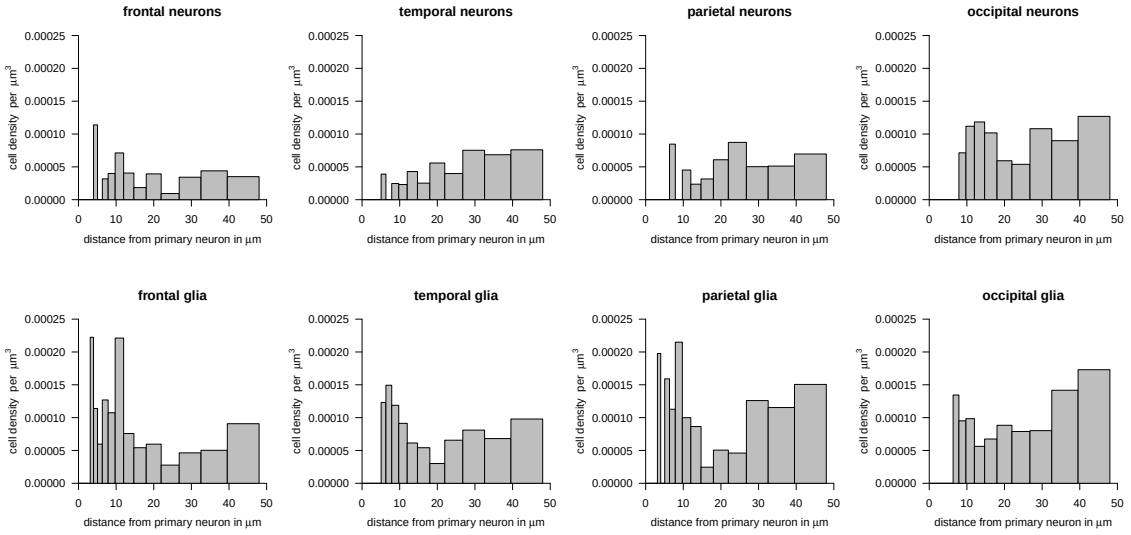

Figure 11: Regional differences in the distribution of neurons and glial cells around primary neurons, radial number density in the four neocortical subregions, frontal, parietal, temporal and occipital cortex. The graphs appear less smooth than in Figure 10 which is probably due to the smaller sample size

density from vertical or isotropic uniform random sections.

Application of the saucor is of course not restricted to neuroscience, but in this field of science it is a particularly valuable tool because it enables the researcher to obtain data on the cellular spatial relations with a reasonable workload and sensitivity which previously were considered difficult to acquire. Even though the saucor is a manual method and the data collection cannot be done by a computer, the labor burden is manageable; the data collection from the brain studied in Section 4 took eight hours per region.

Our results indicate that glia cells are clustered around neurons, whereas neurons showed a tendency towards repulsion from each other. This could be explained with the role of neurons as the morphological, ontogenetical and functional units of the central nervous system, whereas glia cells primarily are the metabolically supportive cells, which assist neurons in their function and development. Although these outcomes are plausible, they are difficult to verify because they were obtained on only one neocortex and there are only few previous studies concerning spatial distribution of cells in healthy human neocortex they could be compared against. Still, the densities found in the present study are within the same ranges as reported earlier for both neurons (Pakkenberg & Gundersen, 1997) and glia cells (Pelvig *et al.*, 2008).

The saucor method also allows analysing the spatial distributions with respect to the size of the primary neurons. Neuron size crudely indicates function (small local interneurons, larger neurons communicating with distant regions in the brain, and very large neurons with axons going far outside the brain). The spatial distributions around neurons of very different sizes are therefore likely to be quite different. This may or may not be interesting in itself, but it represents a known source of variation which may be effectively handled by analysing with respect to a number of size

classes of neurons. Although data on neuron size were collected in the present investigation, we did not include any results since the sample size was too small.

When dealing with tissues like the human neocortex, it would also be interesting to study the layer specific spatial distribution of cells with respect to each other. However, due to the random rotation of the tissue during preparation and the much folded cortical surface it is impossible to identify all six layers in all sections. Knowledge of the 3D spatial relationship between neurons and glial cells may give new insight to the organization and function of the central nervous system, in brains with and without disease. In an earlier pilot study of the human cell distribution in neocortex (Stark *et al.*, 2007), no statistically significant differences were found between healthy male and female brains, nor between young and old brains. This apparent uniformity could be interpreted as an indicator for the importance of spatial arrangement to healthy brain function. Non healthy brains might show a deviation from that spatial distribution pattern. Thus, the radial number density data might provide valuable information when trying to understand the complexity of diseases such as Alzheimer's dementia and schizophrenia where histological data so far have provided only sparse results, but not lead us to fully understand the pathology behind the diseases

Acknowledgements

This work has been supported by the Lundbeck Foundation and by the Danish Council for Strategic Research.

References

Andersen, B. & Gundersen, H. (1999) Pronounced loss of cell nuclei and anisotropic deformation of thick sections. *J. Microsc.*, **196**, 69–73.

Araque, A., Parpura, V., Sanzgiri, R.P. & Haydon, P.G. (1999) Tripartite synapses: glia, the unacknowledged partner. *Trends Neurosc.*, **22**, 208–215.

Baddeley, A.J., Moyeed, R.A., Howard, C.V. & Boyde, A. (1993) Analysis of a three-dimensional point pattern with replication. *Appl. Statist.*, **42**, 641–668.

Baddeley, A. & Jensen, E.B.V. (2005) *Stereology for Statisticians.* Chapman & Hall, Boca Raton, Florida.

Baddeley, A.J., Gundersen, H.J.G. & Cruz-Orive, L.M. (1986) Estimation of surface area from vertical sections. *J. Microsc.*, **142**, 259–276.

Baddeley, A.J., Howard, C.V., Boyde, A. & Reid, S. (1987) Three-dimensional analysis of the spatial distribution of particles using the tandem-scanning reflected light microscope. *Acta Stereol.*, **6**, 87–100.

Berry, M. & Butt, M. (1997) Structure and function of glia in the central nervous system. *Greenfields neuropathology* (edited by D.I. Graham & P. Lantos), pp. 63–83. Oxford University Press, New York.

Chandebois, R. (1976) Cell sociology: a way of reconsidering the current concepts of morphogenesis. *Acta Biotheor.*, **25**, 71–102.

Cressie, N.A.C. (1993) *Statistics for Spatial Data.* John Wiley & Sons, New York, revised edn.

Diggle, P.J. (2003) *Statistical Analysis of Point Patterns.* Arnold Publishers, London, 2nd edition edn.

Dorph-Petersen, K.A., Nyengaard, J.R. & Gundersen, H.J.G. (2001) Tissue shrinkage and unbiased stereological estimation of particle number and size. *J. Microsc.*, **204**, 232–246.

Evans, S.M. & Gundersen, H.J.G. (1989) Estimation of spatial distribution using the nucleator. *Acta Stereol.*, **8**, 395–400.

Hanisch, K.H. & Stoyan, D. (1981) Stereological estimation of the radial distribution function of centres of spheres. *J. Microsc.*, **122**, 131–141.

Horvitz, D.G. & Thompson, D.J. (1952) A generalization of sampling without replacement from a finite universe. *J. Am. Stat. Assoc.*, **47**, 663–685.

Illian, J., Penttinen, A., Stoyan, H. & Stoyan, D. (2008) *Statistical Analysis and Modelling of Spatial Point Patterns.* Statistics in Practice. John Wiley & Sons Ltd., Chichester.

Jensen, E.B., Kiêu, K. & Gundersen, H.J.G. (1990) Second-order stereology. *Acta Stereol.*, **9**, 15–35.

Mattfeldt, T., Frey, H. & Rose, C. (1993a) Second-order stereology of bening and malignant alterations of the human mammary gland. *J. Microsc.*, **171**, 143–151.

Mattfeldt, T., Vogel, U., Gottfried, H. & Frey, H. (1993b) Second-order stereology of prostatic adenocarcinoma and normal prostatic tissue. *Acta Stereol.*, **12**, 203–208.

Mayhew, T.M. (1999) Second-order stereology and ultrastructural examination of the spatial arrangements of tissue compartments within glomeruli of normal and diabetic kidneys. *J. Microsc.*, **195**, 87–95.

Pakkenberg, B. & Gundersen, H. (1997) Neocortical neuron number in humans: effect of sex and age. *J. Comp. Neurol.*, **384**, 312–320.

Pelvig, D.P., Pakkenberg, H., Stark, A.K. & Pakkenberg, B. (2008) Neocortical glial cell numbers in human brains. *Neurobiol. Aging*, **29**, 1754–1762.

Stark, A.K., Petersen, A.O., Gardi, J., Gundersen, H.J.G. & Pakkenberg, B. (2007) Spatial distribution of human neocortical neurons and glial cells according to sex and age measured by the saucer method. *J. Neurosci. Methods*, **164**, 19–26.

Sterio, D.C. (1984) The unbiased estimation of number and sizes of arbitrary particles using the disector. *J. Microsc.*, **134**, 127–136.

Stoyan, D., Kendall, W.S. & Mecke, J. (1995) *Stochastic Geometry and its Applications.* John Wiley & Sons, Chichester, 2nd edn.

Ullian, E., Sapperstein, S., Christopherson, K. & Barres, B. (2001) Control of synapse number by glia. *Science*, **26**, 657–261.

Wiegand, T. & Moloney, K.A. (2004) Rings, circles, and null-models for point pattern analysis in ecology. *Oikos*, **104**, 209–229.